Efficient Terahertz Harmonic Generation with Coherent Acceleration of Electrons in the Dirac Semimetal Cd_{3}As_{2}

Bing Cheng, Natsuki Kanda, Tatsuhiko N. Ikeda, Takuya Matsuda, Peiyu Xia, Timo Schumann, Susanne Stemmer, Jiro Itatani, N. P. Armitage, and Ryusuke Matsunaga

Phys. Rev. Lett. **124**, 117402 — Published 19 March 2020

DOI: 10.1103/PhysRevLett.124.117402

Efficient Terahertz Harmonic Generation with Coherent Acceleration of Electrons in the Dirac Semimetal Cd_3As_2

Bing Cheng[1]†, Natsuki Kanda[2]†, Tatsuhiko N. Ikeda[2], Takuya Matsuda[2], Peiyu Xia[2], Timo Schumann[3], Susanne Stemmer[3], Jiro Itatani[2], N. P. Armitage[1], and Ryusuke Matsunaga[2,4]*

[1]*The Institute for Quantum Matter and Department of Physics and Astronomy, The Johns Hopkins University, Baltimore, MD 21218, USA.*

[2]*The Institute for Solid State Physics, The University of Tokyo, Kashiwa, Chiba 277-8581, Japan.*

[3]*Materials Department, University of California, Santa Barbara, California 93106-5050, USA.*

[4]*PRESTO, Japan Science and Technology Agency, 4-1-8 Honcho Kawaguchi, Saitama 332-0012, Japan.*

†The authors contributed equally.

*e-mail: matsunaga@issp.u-tokyo.ac.jp

We report strong terahertz (~10^{12} Hz) high harmonic generation in thin films of Cd_3As_2, a three-dimensional Dirac semimetal at room temperature. The third harmonics is detectable with tabletop light source and can be as strong as 100 V/cm by applying the fundamental field of 6.5 kV/cm inside the film, showing an unprecedented efficiency for terahertz frequency conversion. Our time-resolved terahertz spectroscopy and calculations also clarify the microscopic mechanism of the nonlinearity originating in the coherent acceleration of Dirac electrons in momentum space. Our results provide clear insights for nonlinear current of Dirac electrons driven by terahertz field under an influence of scattering, paving the way toward novel devices for high-speed electronics and photonics based on topological semimetals.

Realization of intense phase-stable light fields has revealed highly-intriguing nonlinear and nonperturbative light-matter interactions. A prominent example is high harmonic generation (HHG), *i.e.,* the production of coherent high-energy photons by photon-energy multiplication, which has been developed in gaseous media for attosecond science [1] and also utilized for high-resolution angle-resolved photoemission spectroscopy (ARPES) [2]. More recently, HHG in semiconductors with mid-infrared (IR) excitation has been reported [3,4], opening a new route toward laser-based stable and compact soft X-ray sources.

Efficient third harmonic generation (THG) in terahertz (THz) frequency has been also reported in a superconducting film resonating with a collective mode [5]. Realization of such strong THz nonlinearity at room temperature is highly desired for high-speed electronics and for frequency mixing in sensitive detection of far-infrared wave. From this perspective, graphene, a two-dimensional (2D) honeycomb carbon sheet, has attracted tremendous attention because it hosts massless Dirac electrons and their current flow across the Dirac node is expected to exhibit remarkably large nonlinearity [6-13]. The nonlinearity in the current arises from drastic change of electron velocity across the Dirac node under intraband acceleration (See Supplemental Material [14]). THz HHG in graphene has, however, long evaded experimental detection. A signature was first reported in a 45-monolayer graphene at cryogenic temperature [15]. The difficulty of observing THz HHG in graphene has been attributed to fast carrier scattering, which could hamper coherent carrier transport at THz timescales [16], and thus, attention has been shifted to HHG by mid-IR excitation at higher light frequency that exceeds the scattering rate [17-20]. Followed by observation of THz THG in a 2D Dirac system at the surface of a topological insulator [21], very recently the THz HHG in graphene was clearly demonstrated by using very intense light sources based on large accelerators [22]. The nonlinear coefficients in graphene was found to be much larger than typical materials, whereas the conversion efficiency is limited by its monolayer nature. Therefore, realizing higher conversion efficiency in a bulk material is desired for practical application. Another issue to be resolved is the origin of THz HHG in graphene, which was explained by a thermodynamic model where electrons are assumed to be in quasi-equilibrium with repeating heating/cooling processes very rapidly within THz timescale [22,23]. Such a picture of incoherent electron dynamics is an essentially different mechanism from that originally proposed as a source of large nonlinearity in massless Dirac systems [6-13]. A recent time-resolved ARPES for a topological insulator has reported ballistic current of Dirac electrons driven by THz pulse [24]. Getting deeper insight into the microscopic dynamics of Dirac electrons in the high field regime under the influence of scattering is essential as well as is finding other bulk candidates for efficient THz HHG.

In this Letter, we investigate THz nonlinear transmission in thin films of the three-dimensional (3D) Dirac semimetal Cd_3As_2 and report the observation of THz harmonic generation to the extent that it is observable with a tabletop light source at room temperature.

We also perform time-resolved THz spectroscopy to reveal the ultrafast dynamics of Dirac fermions during the THG process. These results provide evidence for the remarkable THz nonlinearity originating from coherent intraband acceleration of Dirac electrons, as shown in Fig. 1(a), which is in good agreement with the calculation including the scattering. Our results provide deeper understanding of Dirac electron current and show the path forward to design efficient frequency-conversion devices that are based on the remarkable features of topological semimetals.

Samples consisting of (112) Cd_3As_2 thin films with 240-nm thickness are epitaxially grown on a GaSb buffer layer on a GaAs substrate [25,26]. The band structure of Cd_3As_2 has two Dirac nodes near the Γ point and quasi-linear band dispersion up to the energy scale of ~1 eV [27,28]. Considering the low concentration and the effective mass of carriers, the Fermi energy E_F is estimated to be as small as ~50 meV above the Dirac nodes [29]. We performed THz time-domain spectroscopy to evaluate the linear response [14]. Figures 1(b) shows the real and imaginary THz conductivity with the fitted results using the Drude model. The scattering time τ_s is 145 fs at 300 K, which is longer than usual metals and graphene. Such long scattering time is often observed in 3D Dirac or Weyl semimetals with prohibited backward scattering [30]. Interestingly, τ_s becomes longer at higher temperature [14], which might be accounted for by the screening of scattering by long-range Coulomb disorders [31-33].

For nonlinear spectroscopy intense THz pulses are generated by the tilted-pulse-front scheme [34,35] with bandpass filters at $f=\omega/2\pi$=0.8 THz [14]. The peak field is 31 kV/cm in atmosphere. Figure 1(c) shows power spectra of the THz pulse after transmitting through the Cd_3As_2 sample. A sharp peak of THG is clearly observed at $3f$=2.4 THz. Clearer data of the fifth harmonics are shown in Supplemental Material [14]. For comparison, we examined monolayer graphene on a SiC substrate with the same excitation condition and also found the THG signal there as well. In contrast, a reference substrate of GaSb/GaAs shows no THG. Figure 1(d) shows the THG field amplitude as a function of the incident fundamental field strength E_{pump}. The data scale as ~E_{pump}^3 for weaker field regimes, but they saturate for stronger excitation, showing nonperturbative behavior. In the perturbative regime for graphene, we estimated the nonlinear coefficient $\chi^{(3)}$ as ~10^{-9} m^2V^{-2}, which is consistent with the previous literature [22] reporting $\chi^{(n)}$ to be 7-18 orders of magnitude larger than typical materials. Compared to graphene, the transmitted fundamental wave for Cd_3As_2 is smaller because of the Fresnel loss; the most part of the incident THz wave is reflected at the metallic surface and only the field of 6.5 kV/cm is applied inside the Cd_3As_2 film. Nevertheless, the detected THG for Cd_3As_2 is stronger than that for graphene, which exhibits much greater conversion efficiency in Cd_3As_2. The THG field amplitude is as strong as 100 V/cm. The Fresnel reflection loss can be avoided by anti-reflection coating on the film or

directly applying the field via contact electrodes, which will generate further stronger harmonics as a realistic frequency conversion for ultrafast electronic application.

To explore the microscopic picture of the efficient HHG mechanism in Cd_3As_2, we performed two types of THz pump-THz probe spectroscopy (TPTP) [5,36,37]. See details in Supplemental Material [14]. Figure 2(a) shows a schematic of TPTP with a broadband short pump pulse with a maximum peak field of 50 kV/cm in air and center frequency of 2 THz. Figure 2(b) shows the probe THz waveform E_{probe} as a function of the probe delay t_2 against the gate pulse for the electro-optic sampling. Figure 2(c) shows a 2D plot of the change of the probe waveform by THz pump, δE_{probe}. With fixing t_2 at the peak of the probe pulse, we plot δE_{probe} as a function of the pump delay t_1 in Fig. 2(d). δE_{probe} grows just after the pump arrives and then decays slowly, indicating dynamics induced by the THz pump. The small dip at t_1~8 ps originates from the reflected THz pump pulse from the back surface of the substrate. Here the probe polarization is perpendicular to the pump ($\boldsymbol{E}_{probe} \perp \boldsymbol{E}_{pump}$), but we confirmed that the result is similar with the case of $\boldsymbol{E}_{probe} \parallel \boldsymbol{E}_{pump}$ [14]. By Fourier transformation, the time-dependent conductivity spectra $\sigma(\omega, t_1)$ are obtained. Figures 2(e) and 2(f) show the real and imaginary parts of $\sigma(\omega, t_1 = 5\ \text{ps})$. Except for the very fast timescale within the pump pulse duration (t_1<2 ps), the conductivity spectra are reasonably fitted by the Drude model, and the fitting parameters of the carrier density N and the scattering time τ_s are plotted in Figs. 2(g) and 2(h) as a function of t_1. The increase of N implies that electrons are excited to the conduction band by the THz pump. According to the increase of the carrier density and electron temperature, τ_s also increases and then slowly decays. It could be accounted for by the screening effect of long-range Coulomb impurity scattering [31-33] and is consistent with the temperature dependence of the equilibrium results [14]. By fitting the relaxation of carrier density with an exponential decay considering multiple reflections of the pump pulses, the relaxation time τ_R was evaluated to be ~8 ps, which is consistent with previous pump-probe studies for Cd_3As_2 with near- and mid-IR excitation [38-40]. In contrast to the case of rapid cooling in graphene (<< 1 ps) [41], the relaxation time τ_R~8 ps in Cd_3As_2 is much longer than the THz field cycle, indicating that, unlike graphene, the rapid heating/cooling cycles do not occur during the THz wave irradiation. In fact, fort this slow relaxation, we performed the thermodynamic-model calculation in Supplemental Material [14] and confirmed that this model cannot reproduce the efficient THG with realistic parameters.

The nonthermal mechanisms of HHG in solids have been discussed in recent literatures in terms of the interband polarization and intraband current [4]. The contribution of interband polarization on HHG, which might be dominant in semiconductors with mid-IR excitation, cannot dominate for THz frequencies since the dephasing time is much shorter than the field cycle and therefore the short-lived polarization cannot emit low-frequency light [42,43]. Note that the interband transition could occur in the Dirac semimetal with supplying additional

population of carriers to contribute nonlinear current. However, the increase of the carrier density observed in Fig. 2(g) was only 20 % even for the broadband intense pump pulse with the center frequency of 2 THz and the peak field of 50 kV/cm. Since E_F~50 meV is larger than the incident THz photon energy (~several meV), the interband transition is not efficient due to the Pauli blocking. For the THG experiment in Fig. 1(c), the interband excitation would be further small because of the lower frequency of 0.8 THz and weaker field strength of 31 kV/cm. Therefore, the results indicate that the interband transition is not a major effect for efficient THG and that the intraband current is the main source of this nonlinearity. A similar situation in a doped Dirac system has been discussed in a previous calculation [12].

To obtain further insight into the *dynamical evolution during the THz THG process*, we also performed another TPTP with quasi-monochromatic pump waveform as schematically shown in Fig. 3(a) (For details, see Supplemental Material [14]). Figure 3(b) shows the pump waveform with f=0.8 THz and the change of the probe field δE_{probe} as a function of t_1 during the pump irradiation. For the case of $\boldsymbol{E}_{probe} \parallel \boldsymbol{E}_{pump}$, an oscillation signal is discerned on the slow-rising incoherent carrier excitation. Figure 3(c) shows its Fourier component with a peak frequency at 1.6 THz. This result means that the THz conductivity oscillates in time with the frequency $2f$ during the pump irradiation. Such a coherent oscillation in pump-probe signal under phase-stable pump field can be observed generally with subcycle time resolution [44]. Note that the "$2f$-oscillation" in the pump-probe signals directly corresponds to the THG in the transmission of the pump because the nonlinear $3f$ current arises from the oscillating conductivity with frequency $2f$, as also studied in superconductors [5] (See more details in Supplemental Material [14]). Importantly, for the case of $\boldsymbol{E}_{probe} \perp \boldsymbol{E}_{pump}$, the $2f$-oscillation signal is hardly seen in time domain and quite small compared to the case of $\boldsymbol{E}_{probe} \parallel \boldsymbol{E}_{pump}$. This is in a stark contrast to the case of superconductors [5], where the $2f$-oscillation was clearly observed in $\boldsymbol{E}_{probe} \perp \boldsymbol{E}_{pump}$; there it is because the *s*-wave order parameter oscillates in time, which results in the isotropic change of the conductivity [45]. If the THG is described by the thermodynamic model [22], the change of the conductivity is also isotropic. Our results for Cd_3As_2 are, however, clearly distinct from these models and shows that the nonlinearity manifests itself almost only for the pump polarization direction. The result can be well explained by the intraband current. When electrons are accelerated by the pump field, the electron distribution function moves rapidly back and forth in the momentum space along with the pump polarization direction, but it appears as if "nothing happens" in other probe polarization directions, which is observed as the anisotropic $2f$-oscillation.

Both of our TPTP experiments strongly indicate that the electrons are quite nonthermal under THz field and therefore the intraband current of accelerated electrons is the main source of the extremely efficient THG. Here we calculated the nonlinear current considering (i) the intraband acceleration in a simple linear dispersion model with τ_s=145 fs and (ii) the

thermodynamic model with τ_R=8 ps [14]. Figure 4(a) shows the HHG spectra for both models with the incident field E_{pump}=31 kV/cm. Figure 4(b) shows the calculated THG amplitudes for both models as a function of E_{pump} in comparison with the experimental data. The intraband acceleration model can reproduce the value of the THG amplitude within the factor of 2 and its saturating behavior even in the simplified model. On the other hand, the thermodynamic model strongly saturates with smaller THG amplitude because the heating piles up due to the long relaxation time, which cannot account for the experimental results.

One might think that such a nonlinear current from accelerated electrons would be significantly suppressed by the scattering since the scattering rate $1/\tau_s$~7 THz is much faster than the pump frequency of 0.8 THz. However, note that even in this case the nonlinear current by coherent acceleration can appear as long as *the electrons are driven into an unbalanced momentum distribution before the scattering*. The comparison between $1/\tau_s$ and f is not important, and we should compare τ_s with the time for building up the unbalanced electron momentum distribution. As an extreme example, when an electric field $E_0 \cos(2\pi f t)$ is applied inside the film, the time required for accelerating electrons from the Fermi surface to the Dirac node can be estimated by the acceleration theorem [14] as

$$t' = \frac{1}{2\pi f} \sin^{-1}\left(\frac{2\pi f}{E_0}\frac{E_F}{e v_F}\right),$$

where v_F=0.93×10^6 m/s is the Fermi velocity [27]. It gives t'~85 fs for E_0=6 kV/cm and E_F=50 meV, which is shorter than τ_s=145 fs. Importantly, t' is not sensitive to the frequency f. Therefore, the electrons are coherently accelerated by several-kV/cm THz field to form a quite nonthermal momentum distribution before the scattering and contribute to the nonperturbative HHG even for the low-frequency driving force.

Figure 4(c) shows the calculated result of the THG amplitude as a function of τ_s for the peak fields of 3 and 6 kV/cm inside the film and f=0.8 THz. If τ_s is longer than ~85 fs, the THG amplitude strongly saturates into the nonperturbative regime and behaves as if in the long-τ_s limit. Therefore, τ_s~150 fs in this material is "long enough" for nonperturbative intraband acceleration driven by a few-kV/cm field. Figure 4(d) shows the 2D plot of electron distribution in the momentum space driven by the field in comparison with equilibrium. A few-kV/cm THz field inside the film induces substantial unbalance of the intraband electron distribution in the pump polarization direction. Note that such a nonthermal population of Dirac electrons driven by a THz field has been also recently demonstrated in a time-resolved ARPES in a topological insulator [24].

In conclusion, we observed the extremely efficient THz THG in the Dirac semimetal Cd_3As_2. Our TPTP experiments as well as the calculations clearly demonstrate that the THz field coherently accelerates Dirac electrons. In spite of the presence of the scattering, several-kV/cm THz field can drive the system into a nonthermal, unbalanced momentum

distribution before the scattering, which generates nonperturbative nonlinear current. Even longer scattering times might be achieved in other topological semimetals with massless dispersion, which will show stronger frequency conversion perhaps in sub-kV/cm field strength. The results in this work opens a new pathway to develop a novel frequency convertor in THz frequency based on Dirac semimetals.

Acknowledgments

The experiment was supported by JST PRESTO (Grant No. JPMJPR16PA) and in part by JSPS KAKENHI (Grants Nos. JP19H01817, JP19K15462, and JP18K13495). R.M. also acknowledges support by MEXT Quantum Leap Flagship Program (MEXT Q-LEAP) Grant Number JPMXS0118068681. B.C. and N.P.A. were supported by NSF EFRI 2-DARE 1542798 and NSF DMR 1905519. N.P.A. acknowledges additional support from the JSPS International Research Fellows Program. T.S. and S.S. acknowledge support through the Vannevar Bush Faculty Fellowship program by the U.S. Department of Defense (Grant No. N00014-16-1-2814).

B. C. and N. K contributed equally to this work.

References

[1] P. B. Corkum andF. Krausz, Nature Phys. **3**, 381 (2007).
[2] T. Kiss *et al.*, J. Elec. Spec. Rel. Phen. **144-147**, 953 (2005).
[3] S. Ghimire, A. D. DiChiara, E. Sistrunk, P. Agostini, L. F. DiMauro and D. A. Reis, Nature Phys. **7**, 138 (2011).
[4] O. Schubert *et al.*, Nature Photon. **8**, 119 (2014).
[5] R. Matsunaga, N. Tsuji, H. Fujita, A. Sugioka, K. Makise, Y. Uzawa, H. Terai, Z. Wang, H. Aoki, and R. Shimano, Science **345**, 1145 (2014).
[6] S. A. Mikhailov, Europhys. Lett. (EPL) **79**, 27002 (2007).
[7] S. A. Mikhailov and K. Ziegler, J. Phys.: Cond. Mat. **20**, 384204 (2008).
[8] A. R. Wright, X. G. Xu, J. C. Cao, and C. Zhang, App. Phys. Lett. **95**, 072101 (2009).
[9] K. L. Ishikawa, Phys. Rev. B **82**, 201402(R) (2010).
[10] F. H. M. Faisal, J. Phys. B: At. Mol. Opt. Phys. **44**, 111001 (2011).
[11] I. Al-Naib, J. E. Sipe, and M. M. Dignam, Phys. Rev. B **90**, 245423 (2014).
[12] I. Al-Naib, M. Poschmann, and M. M. Dignam, Phys. Rev. B **91**, 205407 (2015).
[13] J. L. Cheng, N. Vermeulen, and J. E. Sipe, Phys. Rev. B **91**, 235320 (2015).
[14] See Supplemental Material at …. for our experimental methods, additional data, and theoretical analysis.

[15]. P. Bowlan, E. Martinez-Moreno, K. Reimann, T. Elsaesser, and M. Woerner, Phys. Rev. B **89**, 041408(R) (2014).
[16]. M. J. Paul *et al.*, New J. Phys. **15**, 085019 (2013).
[17]. N. Yoshikawa, T. Tamaya, and K. Tanaka, Science **356**, 736 (2017).
[18]. M. Baudisch *et al.*, Nature Commun. **9**, 1018 (2018).
[19]. T. Jiang *et al.*, Nature Photon. **12**, 430 (2018).
[20]. G. Soavi *et al.*, Nature Nanotech. **13**, 583 (2018).
[21] F. Giorgianni *et al.*, Nature Commun. **7**, 11421 (2016).
[22] H. A. Hafez *et al.*, Nature **561**, 507 (2018).
[23] Z. Mics, K.-J. Tielrooij, K. Parvez, S. A. Jensen, I. Ivanov, X. Feng, K. Müllen, M. Bonn, and D. Turchinovich, Nature Commun. **6**, 7655 (2015).
[24] J. Reimann *et al.*, Nature **562**, 396 (2018).
[25] T. Schumann, M. Goyal, H. Kim, and S. Stemmer, APL Mater. **4**, 126110 (2016).
[26] T. Schumann, M. Goyal, D. A. Kealhofer, and S. Stemmer, Phys. Rev. B 95, 241113(R) (2017).
[27] A. Akrap, M. Hakl, S. Tchoumakov, I. Crassee, J. Kuba, M. O. Goerbig *et al.*, Phys. Rev. Lett. **117**, 136401 (2016).
[28] I. Crassee, R. Sankar, W. L. Lee, A. Akrap, and M. Orlita, Phys. Rev. Mater. **2**, 120302 (2018).
[29] B. Cheng, T. Schumann, Y. C. Wang, X. S. Zhang, D. Barbalas, S. Stemmer, and N. P. Armitage, arXiv:1905.00309 (2019).
[30] C. C. Homes, M. N. Ali, and R. J. Cava, Phys. Rev. B **92**, 161109(R) (2015).
[31] T. Ando, J. Phys. Soc. Jpn. **75**, 074716 (2006).
[32] E. H. Hwang, S. Adam, and S. Das Sarma, Phys. Rev. Lett. **98**, 186806 (2007).
[33] S. V. Syzranov and L. Radzihovsky, Annu. Rev. Condens. Matter Phys 9, 35 (2018) and references therein.
[34] J. Hebling, K.-L. Yeh, M. C. Hoffmann, B. Bartal, and K. A. Nelson, J. Opt. Soc. Am. B **25**, B6 (2008).
[35] R. Shimano, S. Watanabe, and R. Matsunaga, J. Infrared Milli. Terahz. Waves **33**, 861 (2012).
[36] R. Matsunaga and R. Shimano, Phys. Rev. Lett. **109**, 187002 (2012).
[37] R. Matsunaga, Y. I. Hamada, K. Makise, Y. Uzawa, H. Terai, Z. Wang, and R. Shimano, Phys. Rev. Lett. **111**, 057002 (2013).
[38] C. Zhu *et al.*, Nature Commun. **8**, 14111 (2017).
[39] W. Lu, J. Ling, F. Xiu, and D. Sun, Phys. Rev. B **98**, 104310 (2018).
[40] W. Zhang *et al.*, Appl. Phys. Lett. **114**, 221102 (2019).
[41] I. Gierz, J. C. Petersen, M. Mitrano, C. Cacho, I. C. E. Turcu, E. Springate, A.Stöhr, A. Köhler, U. Starke, A. Cavalleri Nature Mater. **12**, 1119 (2013).

[42] D. Golde, T. Meier, and S. W. Koch, Phys. Rev. B **77**, 075330 (2008).
[43] G. Vampa, C. R. McDonald, G. Orlando, D. D. Klug, P. B. Corkum, and T. Brabec, Phys. Rev. Lett. **113**, 073901 (2014).
[44] M. Sabbar, H. Timmers, Y.-J. Chen, A. K. Pymer, Z.-H. Loh, S. G. Sayres, S. Pabst, R. Santra, and S. R. Leone, Nature Phys. **13**, 472 (2010).
[45] R. Matsunaga, N. Tsuji, K. Makise, H. Terai, H. Aoki, R. Shimano, Phys. Rev. B **96**, 020505(R) (2017).

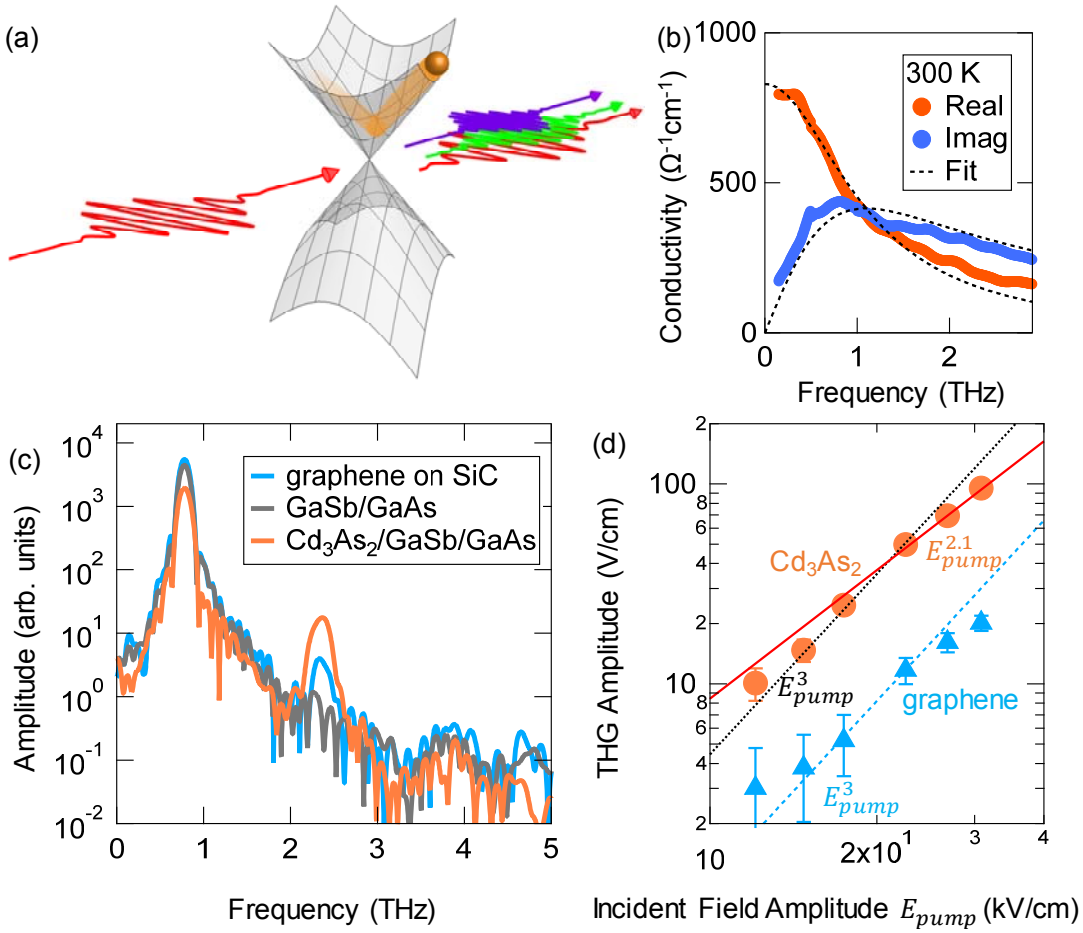

Figure 1. (a) Schematic of the HHG in Dirac electron system. (b) Real- and imaginary-part THz conductivity spectra at 300 K. The dotted curves are the results of fitting. (c) Amplitude spectra of transmitted pump THz pulses for the Cd_3As_2 film, a reference substrate, and graphene on SiC with E_{pump}=31 kV/cm. (d) THG field amplitude as a function of E_{pump}. The solid line for the Cd_3As_2 data is a fitted result with function $\propto E_{pump}^{\alpha}$ with α=2.1 for stronger field. The dashed lines are fitted with $\propto E_{pump}^{3}$ to show the perturbative regimes.

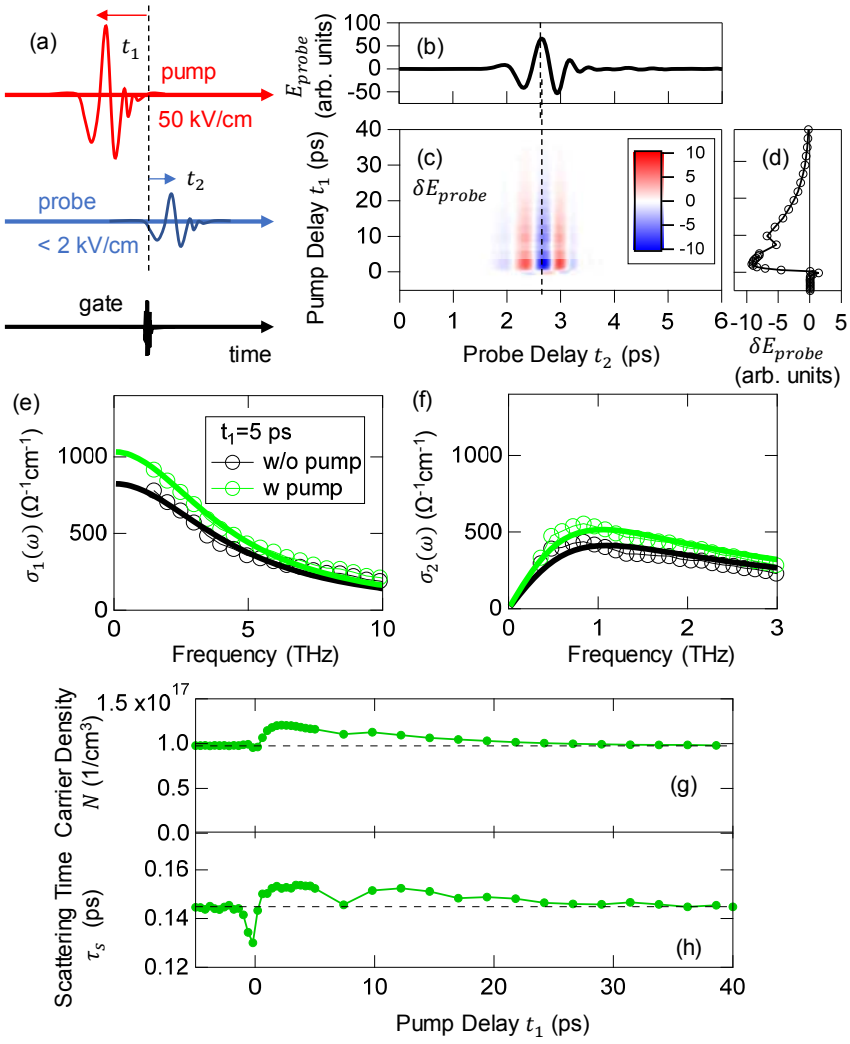

Figure 2. (a) Schematic of broadband short THz pump-THz probe spectroscopy. (b) Probe pulse waveform E_{probe} as a function of t_2. (c) 2D plot of the change of the probe electric field δE_{probe} by the THz pump as functions of t_1 and t_2. (d) δE_{probe} with a fixed delay of t_2 at the peak of the probe indicated by the broken line in (c). (e)(f) Open circles show the real and imaginary parts of the transient conductivity spectra at t_1=5 ps in comparison with data in equilibrium. The solid curves show the fitting with the Drude model. (g)(h) The carrier density N and scattering time τ obtained by the fitting in (e) and (f) as a function of the pump delay t_1.

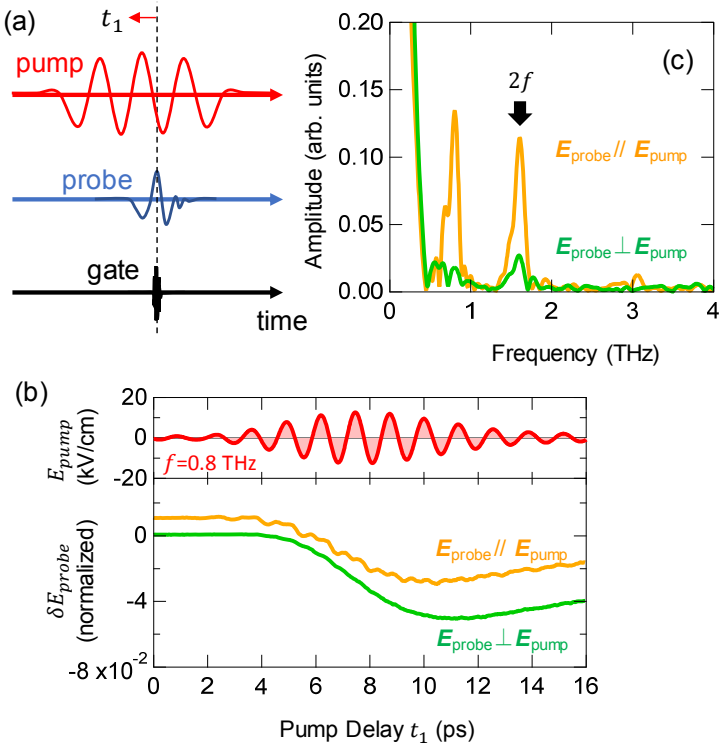

Figure 3. (a) Schematic of quasi-monochromatic THz pump-THz probe measurement. (b) The upper figure shows the pump THz waveform with f=0.8 THz. The lower figure shows δE_{probe} as a function of t_1 for the probe polarizations parallel and perpendicular to the pump. The data are normalized at the peak value of probe field and shown with offset for clarity. (c) Fourier components of δE_{probe} on the interband excitation signal in (b). The arrow indicates the oscillation component at $2f$=1.6 THz. The peak at f=0.8 THz is ascribed to an artifact [14].

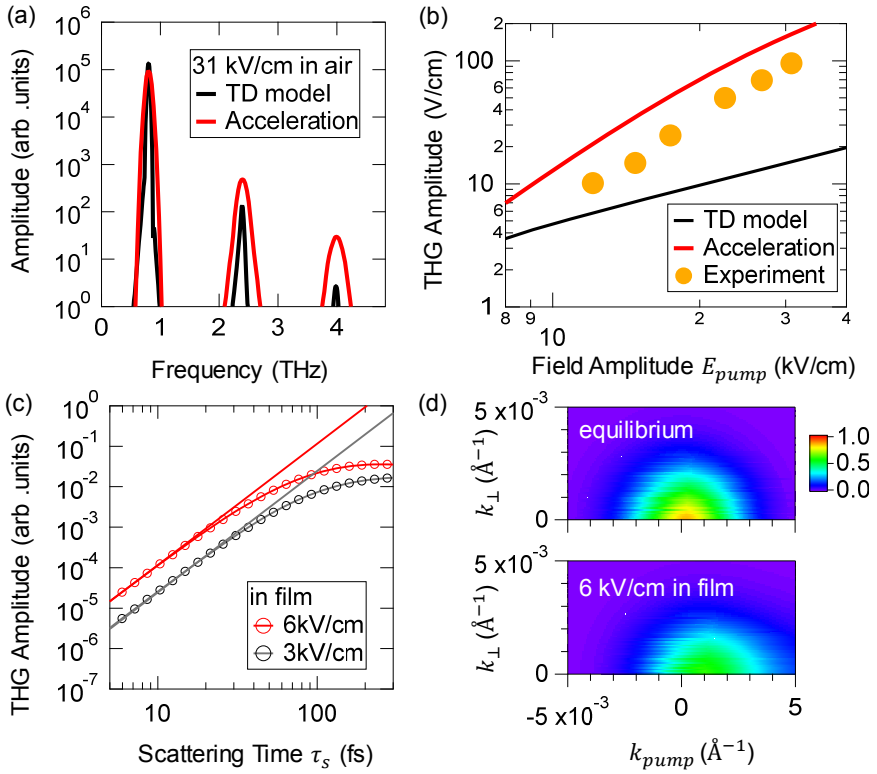

Figure 4. (a) Calculated amplitude spectra from the thermodynamic (TD) model and the intraband acceleration model for f=0.8 THz. (b) THG amplitudes as a function of the field strength. The black and red curves show the results of the TD model and the intraband acceleration model and the circles show the experimental data. (c) THG amplitude as a function of τ_s for f=0.8 THz and peak field of 3 and 6 kV/cm inside the film. The solid lines show power-law fittings to clearly see saturation. (d) 2D plot of the electron distribution in the momentum space parallel and perpendicular to the pump polarization, as denoted by k_{pump} and $k_\perp$, respectively. The top and bottom panels correspond to equilibrium and under the field of 6 kV/cm inside the film at f=0.8 THz.